EUROFUSION WPJET1-PR(16) 16017

V.S. Neverov et al.

Determination of Divertor Stray Light in High-Resolution Main Chamber Ha Spectroscopy in JET-ILW

Preprint of Paper to be submitted for publication in Nuclear Fusion

This work has been carried out within the framework of the EUROfusion Consortium and has received funding from the Euratom research and training programme 2014-2018 under grant agreement No 633053. The views and opinions expressed herein do not necessarily reflect those of the European Commission.

Determination of Divertor Stray Light in High-Resolution Main Chamber H_α Spectroscopy in JET-ILW

V S Neverov[1], A B Kukushkin[1,2], M F Stamp[3], A G Alekseev[1], S Brezinsek[4], M von Hellermann[5], and JET Contributors[6]

EUROfusion Consortium, JET, Culham Science Centre, Abingdon, OX14 3DB, UK
[1]National Research Centre "Kurchatov Institute", Moscow, 123182, Russia
[2]National Research Nuclear University MEPhI, Moscow, 115409, Russia
[3]Euratom/CCFE Fusion Association, Culham Science Centre, Abingdon, Oxon, OX14 3DB, UK
[4]Forschungszentrum Jülich GmbH, Institut für Energie- und Klimaforschung—Plasmaphysik, 52425 Jülich, Germany
[5]ITER Organization, Route de Vinon sur Verdon, St Paul Lez Durance, France
[6]See the appendix of F. Romanelli et al. Proc. 25th IAEA Fusion Energy Conf. (Saint Petersburg, Russia, 2014)

E-mail: vs-never@hotmail.com

Abstract. Theoretical model suggested for ITER Main Chamber H_α Spectroscopy is applied to the high-resolution spectroscopy (HRS) data of recent JET ITER-like wall (ILW) experiments. The model is aimed at reconstruction of neutral hydrogen isotopes density in the SOL, and isotope ratio, via solving a multi-parametric inverse problem with allowance for (i) a strong divertor stray light (DSL) on the main-chamber lines-of-sight (LoS), (ii) substantial deviation of neutral atom velocity distribution function from a Maxwellian in the SOL, (iii) data for direct observation of divertor. The JET-ILW HRS data on resolving the power at deuterium and hydrogen spectral lines of Balmer-alpha series with direct observation of the divertor from the top and with observation of the inner wall along tangential and radial LoS from equatorial ports are analyzed. These data allow to evaluate the spectrum of the DSL and the signal-to-background ratio for Balmer-alpha light emitted from the far SOL and divertor in JET-ILW. The results support the expectation of a strong impact of the DSL upon the ITER Main Chamber H_α (and Visible Light) Spectroscopy Diagnostics.

Keywords: tokamak diagnostics, spectral line shapes, inverse problems

PACS: 52.70.Kz, 52.25.Ya, 32.70.Jz, 02.30.Zz

1. Introduction

The use of an all-metal first wall in future magnetic fusion reactors equipped with a divertor may impose severe limitations on the capabilities of optical diagnostics in the main chamber because of a divertor stray light (DSL) produced by multiple (diffusive and/or mirror) reflections of intense light emitted in the divertor. For optical diagnosis of hydrogen isotopes and various neutral and low ionized impurities

in the far scrape-off layer (SOL) of the main chamber, one should expect strong contribution of the DSL in the same spectral lines. For H_α Spectroscopy Diagnostic in ITER, measurement requirements formulated in ITER Physics Basis [1] stipulate 30% accuracy for the neutral density between the plasma and the first wall, and 20% for the fuel ratio in the edge. The possible impact of the DSL on the measurement accuracy in tokamaks with all-metal first wall was identified later on. On ASDEX Upgrade, the very successful D_α video diagnostic [2, 3] has been based on measuring with a pair of CCD cameras the angle distribution of absolute value of the intensity, integrated in wavelengths within D_α spectral line (i.e. not a high-resolution spectroscopy (HRS)). The inverse problem for reconstructing the 2D profile of D_α emissivity used the data from about 25 000 lines-of-sight (LoS). Unfortunately, after the metallic first wall (tungsten coating) has been installed, this diagnostics is unable to reconstruct the emitting atoms density profile anymore in discharges with high plasma density, because the images have lost the sufficient contrast (see Sec. 4.3 in [2]). Thus, for reliable recovery of sought-for parameters, one has to seek for a proper variability of measurement data not in the images (namely, wavelength-integrated intensity from thousands of LoS), but in the HRS data from few-several LoS.

The first estimates of the DSL (available as ITER Organization internal document), done by S.W. Lisgo (ITER Organization), which took into account only few reflections from the wall, already showed possible importance of the DSL for the H_α diagnostics in ITER. Another limit, namely, multiple reflections for a very high wall reflectivity, which lead to a homogeneous and isotropic distribution of the DSL in the main chamber, was tried in [4], and an analytic model for the Doppler-Zeeman line shape of the DSL was suggested. The ray tracing modelling of the DSL, not resolved in the spectral lines shape, was performed in [5] using the LightTools software. The results of all the above-mentioned works suggested that there may be a substantial dominance of the Balmer-alpha DSL over the Balmer-alpha light emitted from the main chamber SOL (SOL light, SOLL): up to two orders of magnitude for highly reflecting walls (the wall reflection coefficient $R_w \geq 0.5$) and high-power operation. These results were obtained using the spatial distribution of the emissivity in the divertor and the SOL in the flat-top stage of the inductive mode of ITER operation with the fusion gain parameter Q = 10, calculated by the SOLPS4.3 (B2-EIRENE) code [6-8] on an expanded numerical mesh, with allowance for the poloidally resolved recycling from the first wall [9].

To meet the ITER measurement requirements, one needs to develop a detailed assessment of the measurement accuracy for the fuel ratio and the recycling flux from the main-chamber first wall, with allowance for the DSL. The evaluation of the measurement accuracy can be done only in the framework of the approach called the synthetic diagnostic. In this approach, one creates synthetic experimental data by using the results of predictive numerical simulations of the main plasma parameters. The synthetic diagnostic makes it possible to directly compare the "true" values of the sought-for quantities with their values recovered, via solving the respective inverse problems, from the synthetic experimental data. The principles of a synthetic H_α diagnostics in the main chamber of tokamak with a strong DSL are presented in [10]. The novelty of this synthetic diagnostics is that it comprises in a united formalism the treatment of the following problems: (i) the effect of a strong DSL on the signal on the LoS (below we'll also use the term "track") in the main chamber, (ii) the effect of a substantial deviation of the neutral atom velocity distribution function (VDF) from a Maxwellian, in the SOL, on the spectral line shapes on the tracks in the main chamber, and (iii) the inclusion of the data of direct observation of the divertor to the inverse problem of recovering the parameters of the hydrogen in the SOL using the signal on the tracks in the main chamber.

Note that, in [10], the following models are used: (a) the (normalized) spectral line shape (not absolute values of spectral intensity!) of the DSL is described with the model [4]; (b) the spectral line shape asymmetry of the intensity of the emission in the SOL, caused by the non-Maxwellian effects (the net inward flux of relatively fast atoms), is described with the model [11]; and (c) the recovery of main parameters of a non-Maxwellian VDF of neutral hydrogen atoms in the SOL (namely, effective temperatures of Maxwellian and non-Maxwellian fractions and the relative content of the hydrogen isotopes) is carried out using the model [12]. The model [12] in its turn relies on the results of the Ballistic Model [13, 14] for the VDF (in the projection of velocity on the direction normal to the chamber wall and the coordinate along this direction) of the hydrogen neutrals in the SOL. The Ballistic Model is based on the dominant contribution of the ballistic flights of fast neutrals to the hydrogen penetration

from the wall into the plasma. Comparison of this model with the VDF of deuterium neutrals in ITER from stand-alone simulations with the EIRENE code [8] applied on the background distribution of the main plasma parameters (2D spatial profiles of the density, temperature and ionization balance) calculated with the SOLPS4.3 (B2-EIRENE) code showed good agreement [13, 14].

The main goal of the Main Chamber H_α diagnostics in ITER is the recovery of the density of all hydrogen isotopes in the SOL, the flux of the hydrogen neutrals from the wall and the hydrogen isotope ratio in the SOL. On this way, one has first to solve successively a number of intermediate inverse problems, which were presented in [10] and are used in this paper (see Sec. 2).

Already the preliminary results of the theoretical model [4], suggested for the ITER Main Chamber H_α (and Visible Light) Diagnostics, have shown that a test of the elaborated approach on the currently running machines with the all-metal first wall is required to benchmark the analysis method. The model [4] was extended and applied for interpretation of the data from the JET ITER-like wall (ILW) experiments. The obtained results [15, 16] confirmed the importance of non-Maxwellian effects for interpreting the Balmer-alpha emission from the far SOL and suggested the necessity, under condition of a strong DSL, to incorporate in the diagnostics relying on the hydrogen light in the SOL also the data from direct observation in the divertor.

Here, the models and algorithms suggested for ITER Main Chamber H_α Spectroscopy in the form they were used in synthetic H_α diagnostics [10] are applied with few changes described in Sec. 3 to the HRS data of recent JET ITER-like wall (ILW) experiments. The JET-ILW HRS data on resolving the power at deuterium and hydrogen spectral lines of Balmer-alpha series with direct observation of the divertor from the top and with observation of the inner wall along tangential and radial LoS from equatorial ports are analysed. These data allow to evaluate the spectrum of the DSL and the signal-to-background ratio for Balmer-alpha light emitted from the far SOL and divertor in JET-ILW. The paper is organized as follows. The H_α diagnostic measurement scheme at JET is presented in Sec. 2. In Sec. 3, theoretical model [10] is specified for the case of JET-ILW experiments analysed here. A particular problem which substantially influences the accuracy of experimental results interpretation, namely the correlation between the fraction of the Balmer-alpha DSL in the total Balmer-alpha signal in the main chamber and the power of the Balmer-alpha light emitted in the divertor, is analysed in Sec. 4. Main results for the spectrum of the DSL and the signal-to-background ratio for Balmer-alpha light emitted from the far SOL and divertor are presented in Sec. 5. Conclusion and plans for the future work are given in Sec. 6.

2. H_α measurement scheme at JET

We analyse the HRS data on resolving the power in Balmer-alpha deuterium and hydrogen spectral lines from a pair of fibre-fed HRS systems: KSRD and KSRB with spectral resolution = 0.0052 nm/pixel and instrumental FWHM = 0.024 nm. The KSRB tracks (lines of sight) 1-10 and KSRD tracks 1-10 observe, respectively, the outer (LFS) and inner (HFS) divertor from the top (the Zeeman σ-components are filtered out). The KSRB track 11 and 12 observe the inner (HFS) wall from equatorial ports (KSRB track 11 is a radial track at the vertical coordinate Z= ~ +200 mm, targeted at a 200 mm spot which covers partly the inboard poloidal limiter and partly the inner wall cladding tile in the 8^{th} octant; KSRB track 12 is a tangential track at Z=~0, targeted at a similar spot at one side of a beryllium inboard poloidal limiter in the 7^{th} octant, with the angle between the track and toroidal field at inner wall Φ =~35.5^o). Layout of observation tracks in the JET main chamber and divertor is shown in figures 1 and 2, respectively.

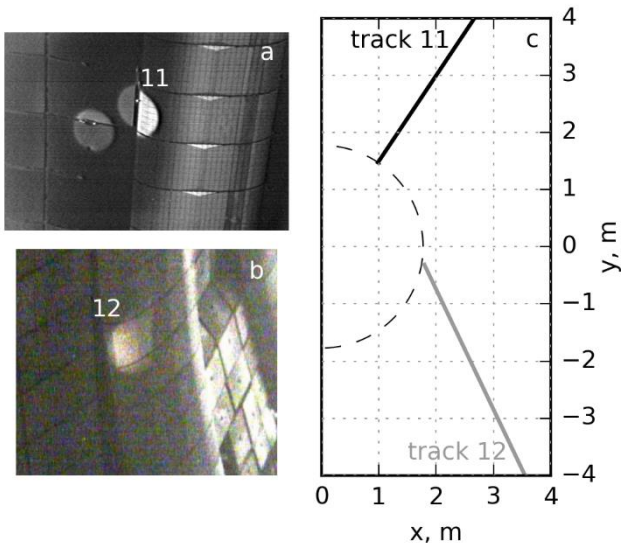

Figure 1. Camera view on the inboard limiter in the 8th octant, the right bright spot is the KSRB track 11 target (a); camera view on the inboard limiter in the 7th octant, the bright spot is the KSRB track 12 target (b); schematic layout (top view) of the KSRB tracks 11 (radial) and 12 (tangential), the dashed line shows the inner wall position in the equatorial plane (c).

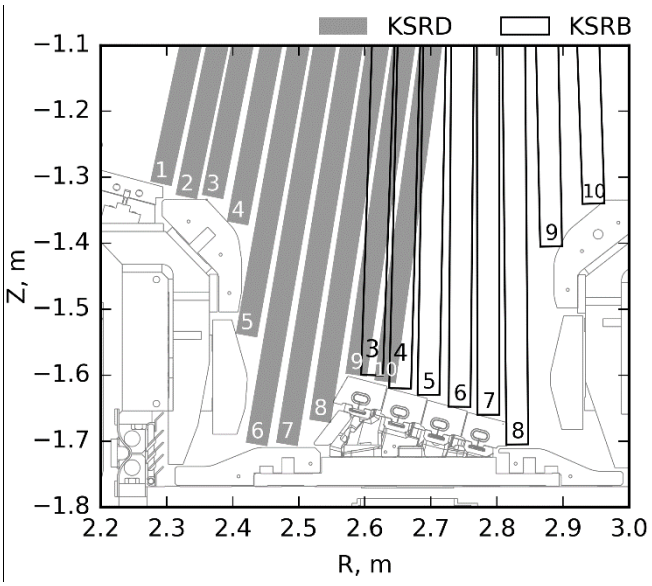

Figure 2. The layout of the KSRD tracks 1 - 10 (grey bars) and the KSRB tracks 3 - 10 (white bars) of the spectrometers viewing from the vessel's top down at divertor. The bars show projections of observation cones on the poloidal plane. The KSRB tracks 1 and 2 are not shown because these lines of sight are presently obstructed.

It is seen in figure 2 that some tracks cross each other, so to model the DSL spectrum we have to choose the tracks which do not intersect in the area of maximum emissivity. We chose KSRD tracks 1 – 9 and KSRB tracks 4 – 10 to model the DSL (16 tracks in total).

The above parameters are valid for the series of pulses considered in the present paper: discharges in deuterium with small admixture of hydrogen, from JET pulse number (JPN) 85752 to JPN 86451, and two discharges in hydrogen with small admixture of deuterium, JPN 87637 and JPN 87638.

3. Theoretical Model

The interpretation of the experimental data is carried out via solving successively the inverse problems of equations (7)-(11), (13)-(20) in [10] for each time interval defined by the exposure time of the spectroscopic equipment. The inverse problems are as follows.

1. Recovering the spatial distribution of the isotope ratio for hydrogen and deuterium and the temperature of the neutral hydrogen isotopes in the divertor from the data on the Balmer-alpha spectral line measurements via direct observation of the divertor.
2. Predictive modelling of the DSL spectral line shape (not the absolute intensity!), based on the results of step 1.
3. Recovering (i) the signal-to-background ratio and (ii) the isotope ratios in the SOL. The task "i" assumes recovering the relative contributions of all three sources to the signal along a track in the main chamber, namely, the light from the low (magnetic) field side (LFS) and high field side (HFS) SOL sections of the track, and the DSL (i.e. the SOLL-to-DSL ratios). Recovering the isotope ratios in the SOL is based on solving a united inverse problem that employs the model for the spectral characteristics of the contributions of the SOL sections and uses the results for the DSL spectral line shape obtained on step 2.

Here we use the formalism of inverse problems described in [10] with the difference that the real experimental data are used instead of the synthetic ones. Note, that the background measured with a blind detector is subtracted from the experimental data prior to solving the inverse problems. The other differences specific to the case of JET-ILW are described below.

We start from the inverse problem for divertor. In JET-ILW, the side components of the Zeeman triplet of the spectral line are filtered out from the signal on the tracks of direct observation of the divertor (see figure 2). In this case the convolution in equation (8) in [10] is needless, and the equation takes a simpler form:

$$S^{\text{theor}}(\lambda_j) = \sum_{t=1}^{M} x_t \sum_{i=\text{H,D,T}} X_i F_{\text{Gauss}}\left(\lambda_j - \lambda_i^{\text{alpha}}, T_t\right) \tag{1}$$

Sometimes the experimental signal may be saturated on the core of the spectral line. Our algorithm would allow one to reconstruct the core of the line shape from the data for the wings of the line shape, however the first constraint in equation (11) in [10] is violated in this case. In this work we do not interpret the data with the saturated signal.

The inverse problem for divertor is solved for the following values of input parameters: $M = 3$, i = H, D for each of ten tracks of the KSRB and KSRD systems (20 tracks in total) using the sequential least squares programming method. The bounds and the default initial guesses for the sought-for quantities are shown in the table 1.

Table 1. The bound and the initial guesses for the sought-for quantities in divertor.

Quantity	Symbol	Bounds	Initial guess
Temperature of the atoms of the fraction *t*	T_t	$0.1\ \ eV \le T_t \le 300\ \ eV$	$(T_1)_0 = 5\ \ eV$ $(T_2)_0 = 25\ \ eV$ $(T_3)_0 = 45\ \ eV$
Partial contribution (statistical weight) of the *t*–th fraction of atoms	x_t	$0 \le x_t \le 1$ (no saturation) $0 \le x_t \le 2$ (saturation)	$(x_t)_0 = 1/3$
Partial contribution of the corresponding hydrogen isotope to the integral intensity	X_i	$0 \le X_i \le 1$	$(X_H)_0 = 0$ $(X_D)_0 = 1$

Note, that the initial guesses shown in table 1 are used only for the first time interval. For the subsequent time intervals, we take initial guesses equal to optimal values of parameters found on the previous time interval.

Also note, that we neglect the asymmetry of the line shape on the tracks of direct observation of the divertor, because this effect, analysed in [17], appears to be small (see figure 10 there).

Equation (13) in [10] is used to calculate the line shape of the DSL without any changes. In this equation the convolution is present, because the polarizing filter is not installed on the KSRB track 11 and 12, and the DSL side components of the Zeeman triplet are not filtered out. Some KSRD and KSRB tracks cross each other, so to model the DSL spectrum we have to choose the tracks which do not intersect in the area of maximum emissivity. We chose KSRD tracks 1 – 9 and KSRB tracks 4 – 10 to model the DSL (K = 16 tracks in total).

For the final inverse problem for main chamber SOL, the first constraint in equation (10) in [10] may be violated in the case of signal saturation (not considered in this work) for the same reason as that for divertor. Although our algorithm can solve the inverse problem for JET-ILW data in the exact form of equations (15)-(20) in [10], in this work we use additional constraint for the characteristic wavelength shift for the spectral contribution of the t-th group of non-Maxwellian atoms, $\Lambda_{t,p}$: $\Lambda_{2,p} = \Lambda_{3,p} \equiv \Lambda_p$, which reduces the number of unknowns without loss of accuracy.

The inverse problem for main chamber SOL is solved for the following input parameters: M = 3, i = H, D for the KSRB tracks 11 and 12 using the sequential least squares programming method. The bounds and the default initial guesses for the sought-for quantities are given in table 2.

Table 2. The bound and the initial guesses for the sought-for quantities in main chamber SOL.

Quantity	Symbol	Bounds	Initial guess
Temperature of the Maxwellian atoms of the fraction t (and effective temperature of the non-Maxwellian atoms of the fraction M+t)	$T_{t,p}$	$0.1\ eV \le T_{1,p} \le 5\ eV$ $1\ eV \le T_{2,p} \le 20\ eV$ $10\ eV \le T_{3,p} \le 300\ eV$	$(T_{1,p})_0 = 2\ eV$ $(T_{2,p})_0 = 15\ eV$ $(T_{3,p})_0 = 70\ eV$
Partial contribution (statistical weigh) of the t–th fraction of atoms	$x_{t,p}$	$0 \le x_{t,p} \le 1$ (no saturation) $0 \le x_{t,p} \le 2$ (saturation)	$(x_{t,p})_0 = \dfrac{1-(x^{\mathrm{DSL}})_0}{6}$
Partial contribution of the t-th non-Maxwellian fraction of atoms	$x_{M+t,p}$	$0 \le x_{M+t,p} \le 1$ (no saturation) $0 \le x_{M+t,p} \le 2$ (saturation)	$(x_{M+t,p})_0 = 0$
Partial contribution of the corresponding hydrogen isotope to the integral intensity	X_i	$0 \le X_i \le 1$	$(X_H)_0 = 0$ $(X_D)_0 = 1$
Characteristic wavelength shift for the spectral contribution of non-Maxwellian atoms	Λ_p	$0.005\ nm \le \Lambda_p \le 0.1\ nm$	$(\Lambda_p)_0 = 0.01\ nm$
Partial contribution of the Zeeman π-component to the total DSL line shape	C_π^{DSL}	$0.3 \le C_\pi^{\mathrm{DSL}} \le 0.38$	$(C_\pi^{\mathrm{DSL}})_0 = 0.33$
Fraction of the DSL in the total signal	x^{DSL}	$0.85(x^{\mathrm{DSL}})_0 \le x^{\mathrm{DSL}} \le 1.15(x^{\mathrm{DSL}})_0$ (track 11)	$(x^{\mathrm{DSL}})_0 = k\dfrac{R_{\mathrm{Total}}^{\mathrm{Div}}}{\{R_{\mathrm{Total}}^{\mathrm{Div}}\}_{max}}$

$0.8\left(x^{\mathrm{DSL}}\right)_0 \le x^{\mathrm{DSL}} \le 1.2\left(x^{\mathrm{DSL}}\right)_0$ (track 12)	$k = 0.47$ (track 11) $k = 0.43$ (track 12)

As it is for the inverse problem for direct observation of the divertor, equations (7), (9)-(11) in [10] and (1) here, the initial guesses shown in table 2 (except that for the last quantity, x^{DSL}) are used only for the first time interval.

The narrow bounds for C_π^{DSL} are suggested by the ray-tracing simulation of the possible DSL line shapes, carried out in NRC "Kurchatov Institute" [18] and to be published elsewhere.

The equation for the initial guess of the last quantity, x^{DSL}, is very important, because it significantly reduces the uncertainty of the recovery of the sough-for parameters. Therefore, this equation as well as the determination of the coefficient k require a detailed presentation, which is given in the next section.

4. The cross-correlation between direct divertor observation data and the DSL

The inverse problem we solve for the KSRB track 11 and 12 has 21 sought-for parameters. To improve the accuracy of the data interpretation it is worth to determine those sought-for parameters which are most conservative for the problem under consideration. At this stage we identified such a parameter which, with a reasonable accuracy, is determined by the geometrical parameters only, namely, vacuum chamber geometry, track layout and detector position in the main chamber. This assumes that the characteristics of the original source of the DSL, which influence the contribution of the DSL to observed signal in the main chamber (i.e. the volume-integrated characteristics, see equation (3) in [10]) weakly depend on the variable spatial distribution of the source in the divertor. If so, one may determine the universal characteristics of the DSL via, first, using a broader database (the data from many discharges in a single inverse problem) and, second, defining the value of the universal characteristics as that recovered with a minimum uncertainty of solving the inverse problems.

We assume that the data of direct observation of the divertor may be used not only to reconstruct the (normalized) spectral line shape of the DSL but also to estimate the reference value of the DSL's fraction in the signal in the main chamber, $(x^{\mathrm{DSL}})_0$, which gives an approximate value relevant at any time moment. The latter may be recovered under the assumption that the $(x^{\mathrm{DSL}})_0$ value on a given track in the main chamber is always, at any time moment, proportional to the wavelength-integrated intensity emitted by the entire divertor, S^{Div}, and inversely proportional to the wavelength-integrated signal on that track in the main chamber, S^{Total}. Thus, the proportionality coefficient, k, is a time-independent quantity and is determined by the vacuum chamber geometry, track layout and detector position. Therefore, unlike the other unknown parameters, this coefficient may be recovered by solving an inverse problem on a large dataset which includes the data from many discharges.

All of the sought-for quantities of tables 1 and 2 as well as the measured signals are formally functions of time whereas the coefficient k is not. Considering the above assumption for $(x^{\mathrm{DSL}})_0$ we have:

$$\left(x^{\mathrm{DSL}}\right)_0(t) = k\frac{R_{\mathrm{Total}}^{\mathrm{Div}}(t)}{\left\{R_{\mathrm{Total}}^{\mathrm{Div}}\right\}_{max}},\quad R_{Total}^{Div}(t) = \frac{S^{\mathrm{Div}}(t)}{S^{\mathrm{Total}}(t)},\quad \left\{R_{\mathrm{Total}}^{\mathrm{Div}}\right\}_{max} = \max_{\{t\in T\}}\left(R_{\mathrm{Total}}^{\mathrm{Div}}(t)\right), \tag{2}$$

$$S^{\mathrm{Div}}(t) = \sum_{l=1}^{K}\frac{S_l^{\exp}(t)R_l}{\sum_{l'=1}^{K}R_{l'}}. \tag{3}$$

where

- $S^{\mathrm{Total}}(t)$ is the total wavelength-integrated Balmer-alpha line intensity at time t measured on a given track (KSRB track 11 or 12);
- $S^{\mathrm{Div}}(t)$ is the wavelength-integrated Balmer-alpha intensity at time t, averaged over the divertor volume (summation in (3) goes over the $K = 16$ tracks: KSRD tracks 19 and KSRB tracks 4 - 10);

- R_l is the major radius of the point of intersection of the track l with the first wall (see the explanation below);
- $\{R_{\text{Total}}^{\text{Div}}\}_{max}$ is the maximum value of $R_{\text{Total}}^{\text{Div}}$, measured on JET during the series of pulses under consideration, namely, from JPN 85752 to JPN 86451. This value was registered at time t = 53.35 s for the pulse 85853 for the KSRB track 11 and at t = 50.05 s for the pulse 86381 for the KSRB track 12.

Note, that to calculate the wavelength-integrated intensity, averaged over the divertor volume, one has to reconstruct the 2D profile of emissivity in the divertor, that is not possible without tomography diagnostics, such as that of ASDEX Upgrade [2,3]. However, since the emissivity profile usually has its maximum not far from the first wall, the width of the cones near the point of their intersection with the first wall are almost equal for all tracks and the line of sight is directed almost from top to down, the values of $S_l^{\exp}$ may be weighted with the major radii of the points of intersection of the tracks with the first wall to approximately calculate the value of $S^{\text{Div}}(t)$. This procedure uses the toroidal symmetry and integrates the volumes of the toroids obtained by the toroidal rotation of the poloidal cross-section of the observation cones in the divertor region.

Since $S^{\text{Total}}(t)$ and $S^{\text{Div}}(t)$ are the known quantities, determination of k for the given track also determines $(x^{\text{DSL}})_0$ for this track.

The optimal value of k may be determined by solving the following inverse problem:

$$\hat{k} = \underset{k}{\operatorname{argmin}}\{f_{mean}(k)\} \tag{4}$$

$$f_{mean}(k) = \langle \hat{f}(k,t) \rangle_t \tag{5}$$

$$\hat{f}(k,t) = f\left(k, \hat{\mathbf{x}}(k,t), \hat{\mathbf{T}}(k,t), \hat{\mathbf{\Lambda}}(k,t), \hat{C}_H(k,t), \hat{C}_\pi^{\text{DSL}}(k,t)\right) \tag{6}$$

$$f \equiv \sum_{j=1}^{N} \left(\tilde{S}^{\exp}(\lambda_j) - S^{\text{theor}}(\lambda_j)\right)^2 \tag{7}$$

where f is the objective function of the inverse problem (15)-(20) in [10], the cap "^" indicates the optimal values of the quantities, the values of $\hat{\mathbf{x}}, \hat{\mathbf{T}}, \hat{\mathbf{\Lambda}}, \hat{C}_H, \hat{C}_\pi^{\text{DSL}}$ are found by solving the inverse problem (15)-(20) in [10], brackets $<\ldots>_t$ mean averaging over time.

Note that $\hat{\mathbf{x}}, \hat{\mathbf{T}}, \hat{\mathbf{\Lambda}}, \hat{C}_H, \hat{C}_\pi^{\text{DSL}}$ depend not only on time, t, but also on k, because they take different values for different values of k.

We selected the following 20 pulses for data processing: 85853, 85854, 85845, 85847, 85843, 85855, 85831, 85848, 85883, 85859, 85882, 86374, 86372, 86378, 86366, 86375, 86368, 86367, 86363, 86377. All these pulses share the same properties:

- significant (> 1 MW) neutral beam injection (NBI) power;
- highest $R_{\text{Total}}^{\text{Div}}$ ratio among pulses 85752 – 86451 either on KSRB track 11 (first ten pulses in the bunch) or on KSRB track 12 (last ten pulses in the bunch).

The inverse problem (15)-(20) in [10] (with respect to the bounds and the initial guesses presented in table 2) was solved for each time moment, t, of the 20 selected pulses for the 15 different preset values of k for each of two tracks. This generated the dataset of the optimal values $\hat{\mathbf{x}}(k,t)$, $\hat{\mathbf{T}}(k,t)$, $\hat{\mathbf{\Lambda}}(k,t)$, $\hat{C}_H(k,t)$ and $\hat{C}_\pi^{\text{DSL}}(k,t)$ for the sought-for quantities and, respectively, for the objective function, $\hat{f}(k,t)$. For each track for each value of k this dataset consists of about 7000 time moments from 20 different pulses. About 4100 and 3700 time moments for each value of k remained for KSRB tracks 11 and 12, respectively, after filtering out the time moments for which the values of $\hat{x}^{\text{DSL}}(k,t)$ on a given KSRB track (11-th or 12-th) are low: $\hat{x}^{\text{DSL}}(k,t) < 0.1k$, and for which the values of $\hat{f}(k,t)$ are too high, because the measured signals are too low and consequently too noisy. Then the values of $f_{mean}(k)$ were calculated for each of two tracks. These values are shown in figure 3. It is seen that for both KSRB tracks 11 and 12 there is an interval on the k axis for which the function $f_{mean}(k)$ is non-monotonic

and has several local minima close to the global one. This region, shown with the dashed lines, defines the uncertainty interval for the optimal value of k. The results we get for the optimal value of k and the uncertainty intervals are presented in table 3. While the optimal value of k determines the value of $(x^{\mathrm{DSL}})_0$ at any time moment, the uncertainty interval for k determines both the bounds (see table 2) and errors (see figures 8 and 12) for x^{DSL}.

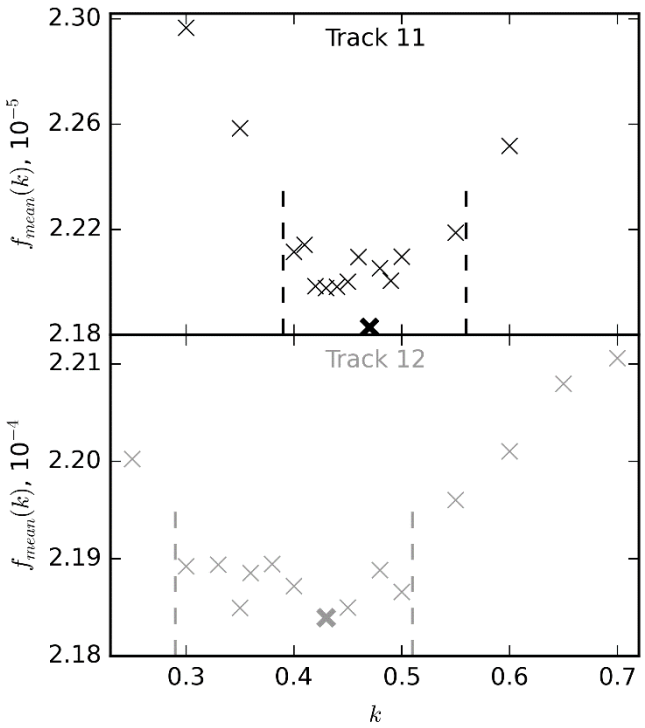

Figure 3. Calculated values of $f_{mean}(k)$ for KSRB tracks 11 (top) and 12 (bottom). The global minimum is marked with bold cross. Dashed lines show the uncertainty interval.

Table 3. Optimal value of the coefficient k in (2).

Track #	Optimal value	Uncertainty interval
11	$\hat{k} = 0.47$	$0.4 < k < 0.55$
12	$\hat{k} = 0.43$	$0.3 < k < 0.5$

5. Main results of JET-ILW data interpretation

While many pulses were analysed, here we present the results only for two pulses: JPN 85853 is the pulse in deuterium with small admixture of hydrogen, and JPN 87638, the pulse in hydrogen with small admixture of deuterium. The first pulse is characterized by up to 12 MW neutral beam injection (NBI) and up to 5 MW ion cyclotron resonance heating (ICRH) power. Also, as noted in Sec. 4, this pulse has the highest value of $R^{\mathrm{Div}}_{\mathrm{Total}}$, which determines approximately the level of the DSL, within the series of pulses from JPN 85752 to JPN 86451. Time evolution of the main parameters for JPN 85853 is shown in figure 4. These parameters include: plasma current (I_p); toroidal field (B_{tor}), electron density (N_{e0}) and electron temperature (T_{e0}) on the magnetic axis; auxiliary heating power of NBI (P_{aux}^{NBI}) and ICRH (P_{aux}^{ICRH}); D_2 and H_2 gas injection rates and the gaps between the separatrix and the inner and outer limiters (designated as RIG and ROG, respectively, and provided by the EFIT code [19] simulations).

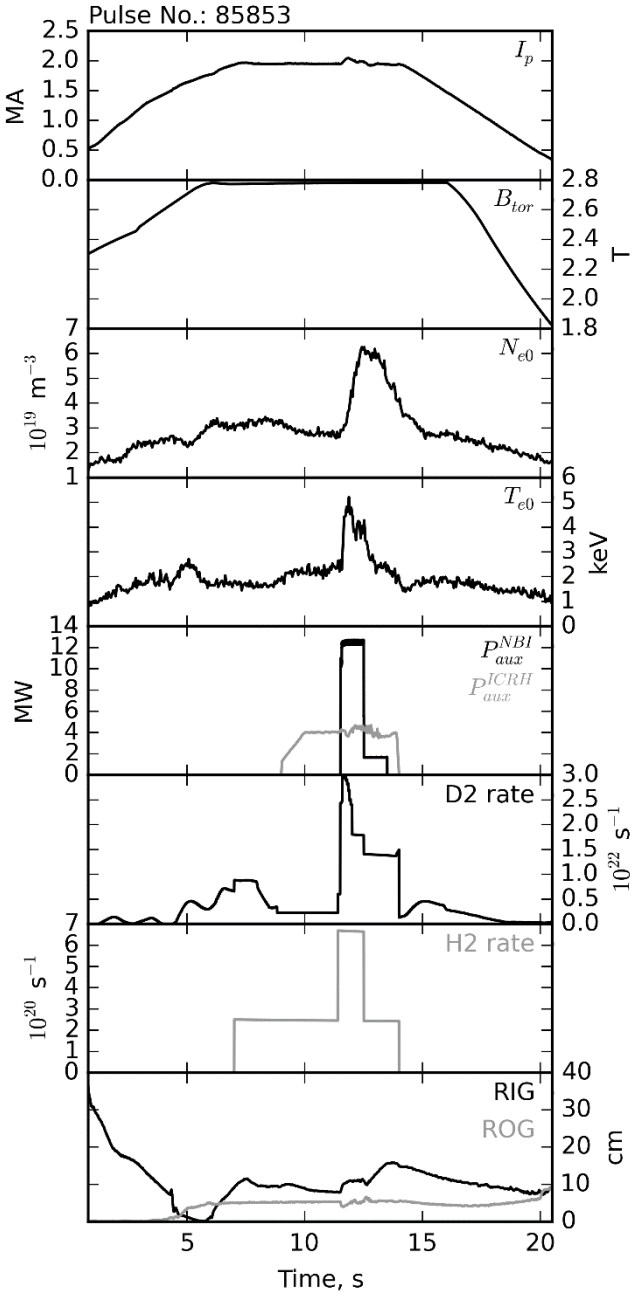

Figure 4. Time evolution of the main parameters for JPN 85853. Notations: I_p is plasma current; B_{tor} , toroidal field on magnetic axis; N_{e0} and T_{e0} , electron density and electron temperature on the magnetic axis; P_{aux}^{NBI} and P_{aux}^{ICRH}, auxiliary heating power for neutral beam injection and ion cyclotron resonance heating, respectively; D2 rate and H2 rate, the D_2 and H_2 gas injection rates; RIG and ROG, the gaps between the separatrix and the inner and outer limiters, respectively (provided by the EFIT code).

Figure 5 shows the results of fitting the signals measured at 13.4 s in JPN 85853 by the KSRD tracks 1 – 9 and the KSRB tracks 4 - 10, which provide the direct observation of the divertor. This stage of the pulse is characterized by the high power D_α radiation near the divertor plates, which can be seen in the CCD camera images as well. The values of relative residual ΔS (8), weighted with the normalized distribution of the spectral intensity, are presented:

$$\Delta S = 100\% \cdot \sum_{j=1}^{N} \left| 1 - \frac{S^{\text{theor}}(\lambda_j)}{\tilde{S}^{\text{exp}}(\lambda_j)} \right| \frac{\tilde{S}^{\text{exp}}(\lambda_j)}{\sum_{j'=1}^{N} \tilde{S}^{\text{exp}}(\lambda_{j'})} \equiv 100\% \cdot \frac{\sum_{j=1}^{N} \left| \tilde{S}^{\text{exp}}(\lambda_j) - S^{\text{theor}}(\lambda_j) \right|}{\sum_{j'=1}^{N} \tilde{S}^{\text{exp}}(\lambda_{j'})} \tag{8}$$

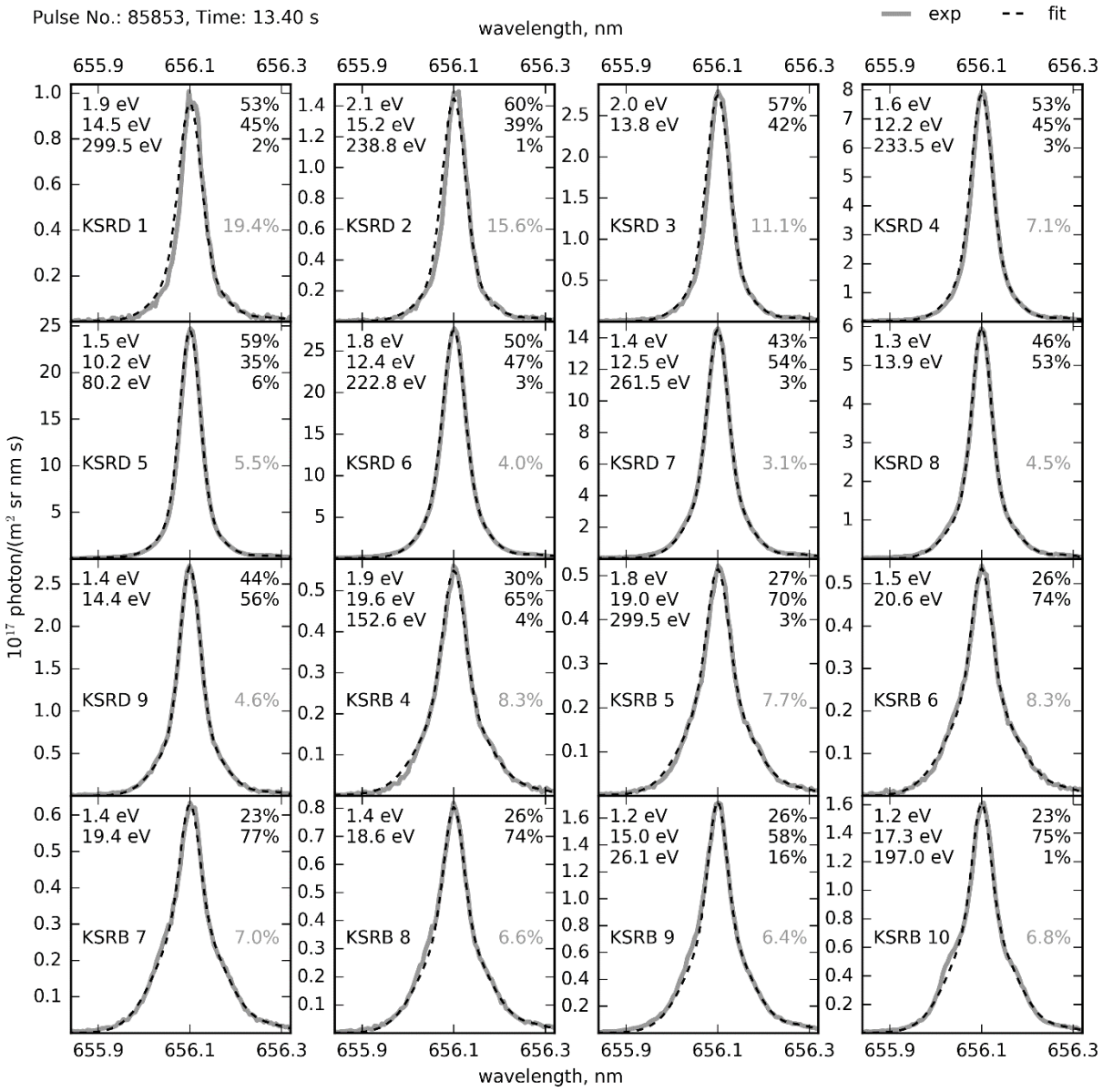

Figure 5. Fitting the experimental signals measured in JPN 85853 at 13.4 s. on the KSRD tracks 1-9 and the KSRB tracks 4-10 of direct observation of the divertor, by solving the inverse problem (see equations (7)-(11) in [10], (1) and table 1). The recovered values of the temperatures T_t are given in the left top corner of each plot, and the respective values of x_t are shown in the right top corner. The values of relative residual ΔS (8) are shown in each plot in grey.

One can notice that the left wing of the experimental spectrum is not perfectly fitted with the theoretical spectrum for the KSRB tracks 7 – 10. This is the result of the small asymmetry of the line shape, neglected (as stated above) in the model for the direct observation of the divertor.

Figure 6 shows the results of fitting the spectra on the KSRB track 11 (radial), which observes the main chamber, for four different time moments of JPN 85853. At 1.6 s. the LFS SOLL fraction dominates in the signal, while at 5.15 s. the HFS SOLL fraction does. This correlates both with the RIG and ROG parameters shown in figure 4 (the smaller the value of RIG/ROG, the higher is the HFS/LFS fraction in the signal) and with the visual information from the CCD camera images. Note, that RIG and ROG are

used in the fitting algorithm only to calculate the values of Zeeman splitting for HFS and LFS SOLL spectra and are not used to recover the respective fractions. At 8.75 s, the recovered DSL fraction in the signal appears to be 20% and increases to almost 40% at 13.4 s. Note, that the error of recovering the effective temperatures is not estimated: in our opinion, in such a complicated inverse problem with so many free parameters this error may be substantially higher than that estimated in [17] where the synthetic (not real experimental) data for divertor were analysed in the framework of similar inverse problem but with only 9 free parameters, cf. figures 12 and 13 in [17].

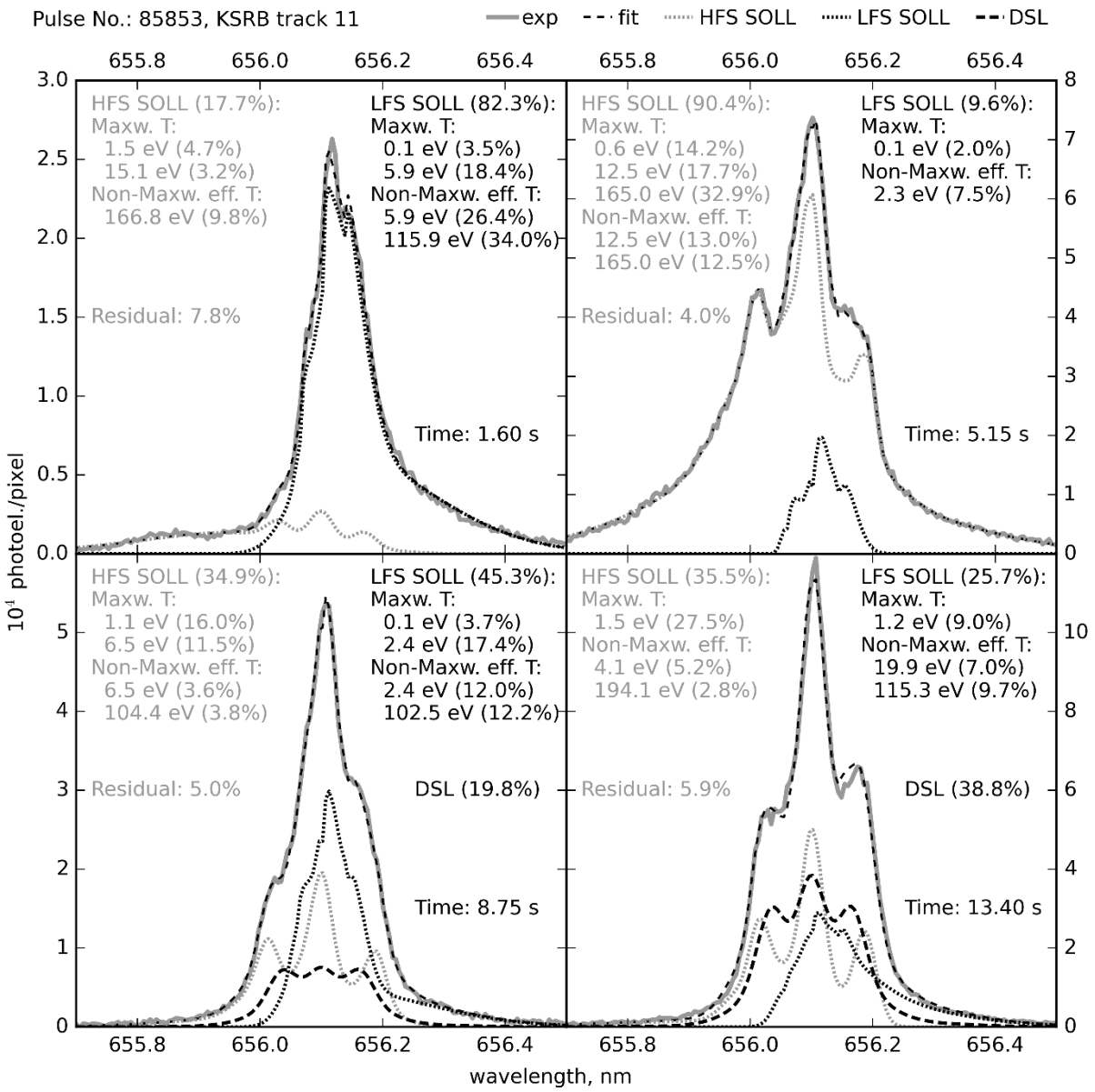

Figure 6. The results of fitting the spectra on the KSRB track 11 (radial) for four different time moments of JPN 85853. The recovered spectral contributions of all three possible sources of light (HFS SOLL, LFS SOLL and DSL) and their fractions in the total signal are shown. The temperatures of atomic fractions and their partial contributions (shown in brackets) to the total observed intensity are indicated for HFS and LFS sections of the SOL. The values of relative residual ΔS (8) are shown in each plot on the left.

Figure 7 shows the results of fitting the spectra on the KSRB track 12 (tangential) of observation of the main chamber. One might expect that the more symmetric line shape as compared to that for the KSRB track 11 should significantly simplify the fitting, however this track does not collect enough photons most of the time, that results in a too noisy signal. Only two time moments from figure 6 are shown in figure 7, because at 1.6 s. and at 8.75 s. the signal on the KSRB tracks 12 is too low to get confidential

results. As it is for the KSRB track 11, the HFS SOLL dominates in the signal at 5.15 s. and the fraction of the HFS SOLL in the total signal is slightly higher than that of the LFS SOLL at 13.4 s. However, the fraction of the DSL is almost 2 times lower for the KSRB track 12 than that for the KSRB track 11 at 13.4 s.

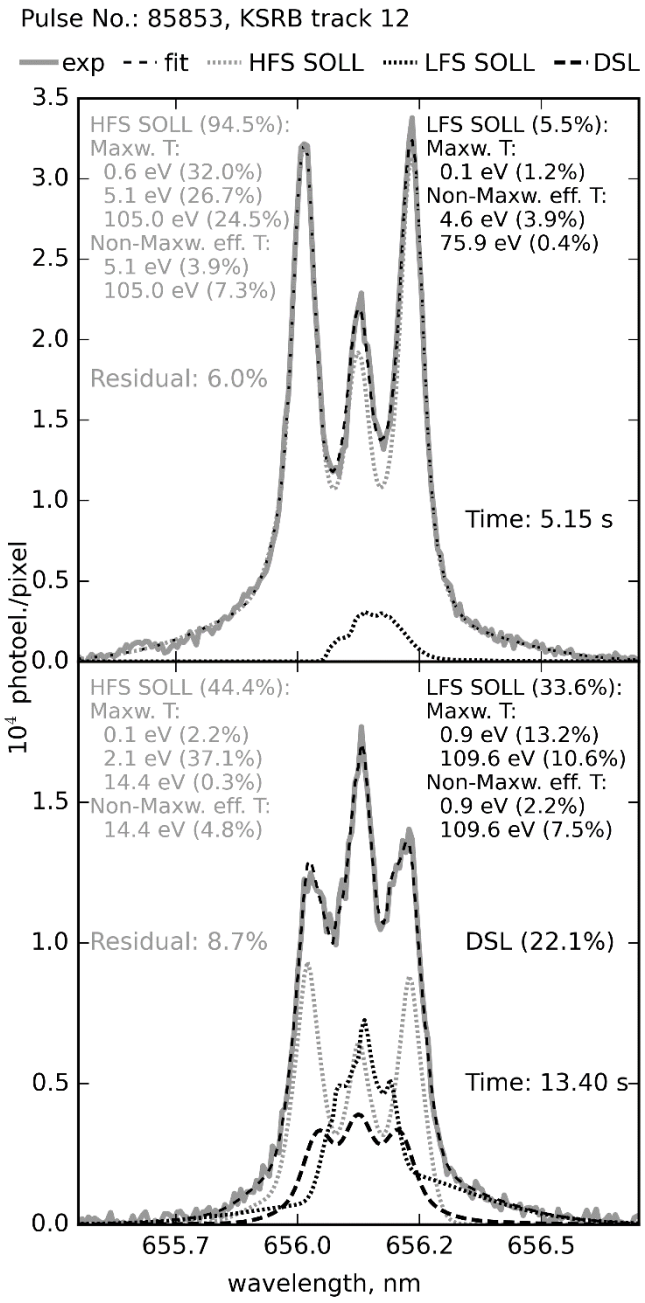

Figure 7. The results of fitting the spectra on the KSRB tracks 12 for two different time moments of JPN 85853. See the caption of figure 6 for the details.

The main results obtained for JPN 85853 are shown in figure 8. This figure shows, for the KSRB track 11, the time evolution of the recovered partial contributions of various sources of light (HFS SOLL, LFS SOLL, DSL) to the integral intensity. The error for DSL fraction is relative and determined by the uncertainty of the coefficient *k* (see figure 3 and table 3). It is about ±15% for the KSRB track 11. The error of HFS and LFS SOLL fractions recovery was analysed in [10] in the frame of the same inverse problem using the synthetic data of ITER operation. Nevertheless, one may expect that in JET the *absolute* errors of recovering the HFS and LFS SOLL fractions may be similarly to ITER be as high as

± 0.2 even for negligible spectrometer noise. It is shown in [10] that the algorithm tends to underestimate the recovered HFS/LFS SOLL fraction if the "true" value is above 0.8 and to overestimate the respective fraction if the "true" value is below 0.2. It is important to note that the reliable evaluation of measurement errors needs direct comparison of recovered and "true" values. The latter needs generating the synthetic data for spectral emissivity in the main chamber and divetor in JET, similarly to the analysis [10] for ITER.

The wavelength-integrated Balmer-alpha intensity, averaged over the divertor volume, $S^{Div}(t)$ (3) is shown to illustrate the correlation between the divertor emission and the recovered fraction of the DSL in the total signal on the KSRB track 11. It appears that the HFS SOLL fraction in the signal correlates with the RIG parameter shown in figure 4 and duplicated in figure 8. A decrease of the RIG parameter leads to an increase of the HFS SOLL fraction.

The results of figure 8 are presented only for the KSRB track 11, because, as mentioned above, confident results for the KSRB track 12 may be obtained only in the very limited range of time moments of JPN 85853.

Figure 9 shows time evolution of the recovered value of small hydrogen fraction in the H+D mixture in the divertor and the SOL for JPN 85853. The hydrogen fraction in the divertor is averaged over the results of recovery from the data for the KSRD track 1 – 9 and the KSRB tracks 4 – 10. The averaging is defined as follows:

$$\left[\frac{H}{H+D}\right]_{Div}(t) = \sum_{l=1}^{K} \frac{\left[\frac{H}{H+D}\right]_l (t) R_l}{\sum_{l'=1}^{K} R_{l'}}. \tag{9}$$

The data for KSRB track 12 have the highest spread of recovered values because of the very noisy signal on the track. Based on the spread of values the absolute error for H/(H+D) recovery may be estimated as ±0.04 for KSRB track 12, ±0.02 for KSRB track 11 and only ±0.01 for divertor. The spread of values for divertor data is low not only because of averaging in (9), but also because the inverse problem is much simpler as compared to that for SOL.

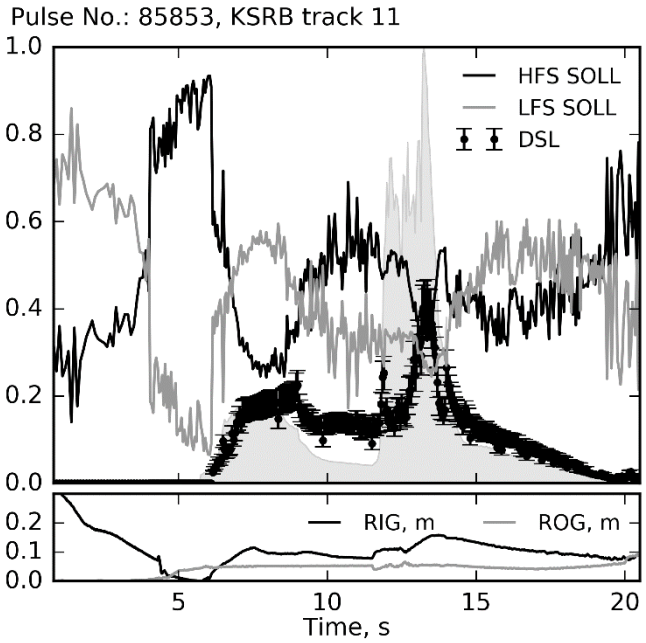

Figure 8. Time evolution of partial contributions of various sources of light (HFS SOLL, LFS SOLL, DSL) to the integral intensity observed on the KSRB track 11 for JPN 85853. $S^{Div}(t)$ (3) is shown with grey background. RIG and ROG parameters (see figure 4) are shown juxtaposed to illustrate the correlation.

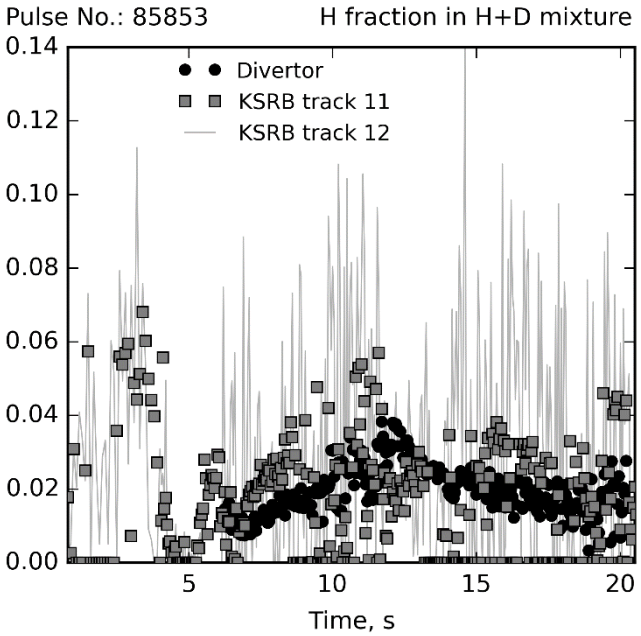

Figure 9. Time evolution of the H/(H+D) ratio in the divertor (volume-averaged, using the KSRB and KSRD divertor direct observation data) and in the SOL (KSRB tracks 11 and 12), recovered for JPN 85853.

Figure 10 shows time evolution of main parameters of JPN 87638 with hydrogen plasma. NBI heating is off for this pulse. No data for D_2 injection rate are available.

Figure 11 shows the results of fitting the spectra on the KSRB track 11, at 4.1 s. and at 13.9 s. of JPN 87638. At 4.1 s the HFS SOLL fraction in the total signal is 1.5 times higher than that of the LFS SOLL. The emissivity of plasma near both the inner and the outer limiters is clearly visible in the CCD camera images at this time moment. The fraction of about 16% of the DSL is present in the signal at 13.9 s. One can notice from figure 11, that the H_α line shape looks smoother than that of D_α. This is so, because the FWHM of Doppler broadening for H_α line is $\sqrt{2}$ times greater than that for D_α line for the same temperature of atoms.

Time evolution of the recovered partial contributions of HFS SOLL, LFS SOLL and DSL to the integral intensity are shown in figure 12 for JPN 87638 for the KSRB track 11. One can notice a correlation between the HFS SOLL fraction in the total signal and the RIG parameter shown in figure 10 and duplicated in figure 12. For JPN 87638, the DSL affects the measurements in the main chamber not so much as it does for JPN 85853.

Figure 13 shows time evolution of the recovered value of small deuterium fraction in the H+D mixture in the divertor and the SOL for JPN 87638. This fraction appears to be a few percent only.

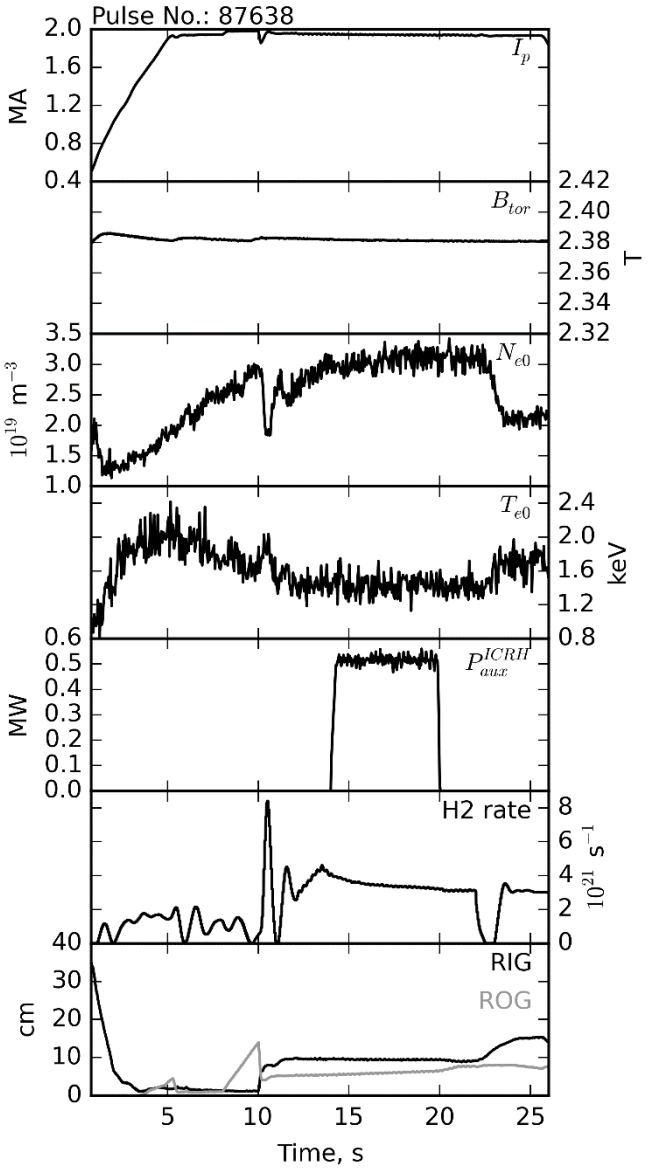

Figure 10. Time dependence of main parameters for JPN 87638. See the caption for figure 4 for the notations.

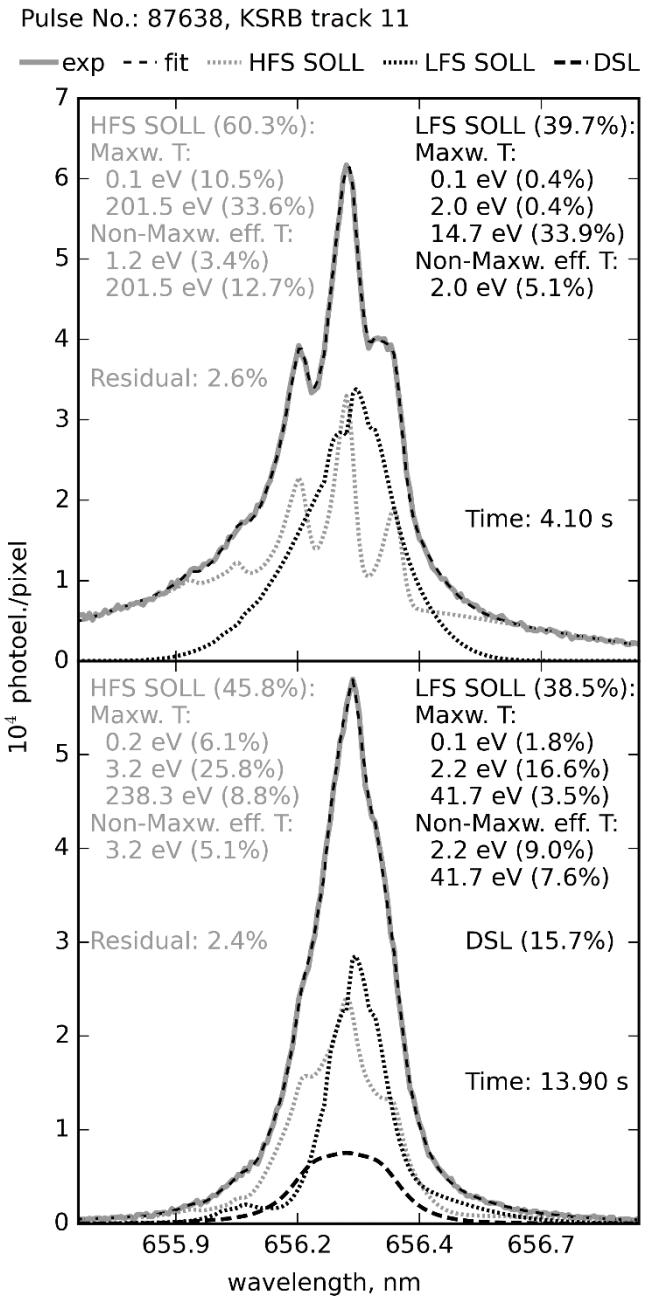

Figure 11. The results of fitting the spectra on the KSRB tracks 11 for two different time moments of JPN 87638. See the caption for figure 6 for the details.

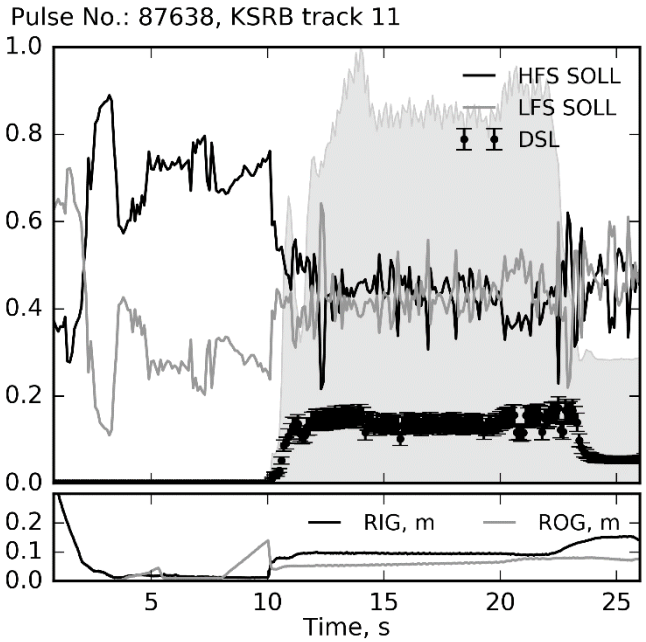

Figure 12. Time evolution of partial contributions of various sources of the light to the integral intensity observed at the KSRB track 11 for JPN 87638. See the caption for figure 8 for the details.

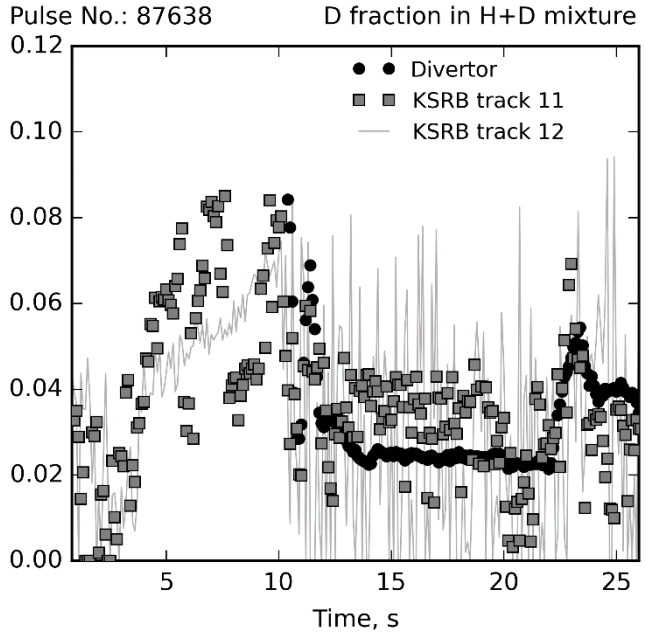

Figure 13. Time evolution of the D/(H+D) ratio in the divertor (volume-averaged, using the KSRB and KSRD divertor direct observation data) and in the SOL (KSRB tracks 11 and 12), recovered for JPN 87638.

6. Discussion, conclusions

The deuterium and hydrogen Balmer-alpha line high-resolution spectroscopy (HRS) data from JET-ILW experiments are interpreted with the algorithms [10] developed for the H_α (and Visible Light) Spectroscopy Diagnostic in ITER. This enabled us to evaluate (i) the shapes of the spectra of the light emitted from the far SOL (SOL light, SOLL) and divertor, with the divertor emission being observed directly from the main chamber's top and as a divertor stray light (DSL) on the lines of sight (LoS) in

the main chamber in the nearly equatorial planes, and (ii) the ratio of respective wavelength-integrated intensities (SOLL/DSL). The results enable us to draw the following conclusions.

1. It is necessary to take into account that both the HFS and LFS SOLL may contribute to the signal in the main chamber on any stages of the discharge. In particular, the results show that the contribution of the LFS SOLL may be higher than that of the HFS SOLL when the plasma is detached from the limiters.

2. The uncertainty of solving the inverse problems to recover the DSL/SOLL ratio is appreciably reduced thanks to assumption that the DSL/SOLL ratio should be proportional to the ratio of the total power of divertor emission to the intensity measured on the LoS in the main chamber. The proportionality coefficient should depend on the geometrical parameters only and is independent of time. This assumption and the recovery of the proportionality coefficient from data for many pulses enabled us to improve the stability of solving the inverse problems and thus decrease the spread of the results for the DSL/SOLL ratio by several times as compared to [15].

3. As compared to [16], the algorithm is improved to handle the discharges with any H/D ratio and not only those with a small admixture of hydrogen in deuterium. This enables us to analyse the pulses in hydrogen.

4. Within the analysed series of pulses in deuterium: from JPN 85752 to JPN 86451, the maximum recovered value of DSL/SOLL is ~ 0.9 for the KSRB track 11 (radial) and ~ 0.8 for the KSRB track 12 (tangential). These values are few times smaller than those obtained in [15] for JPN 83624, however, it is not possible to analyse JPN 83624 with improved algorithm, because the KSRD spectrometer, which data is required to simulate the DSL spectrum, was not set to D_α wavelength. For the two analysed pulses in hydrogen: JPN 87637 and JPN 87638 the DSL/SOLL ratio ≤ 0.25. More analysis is needed to identify the dependence of the DSL/SOLL on the divertor radiation power, recycling level, degree of detachment, divertor configuration, etc.

5. The results show the importance of non-Maxwellian effects (and respective asymmetry of the line shape) in the interpretation of the Balmer-alpha high-resolution spectroscopy (HRS) data.

6. On the whole, the results for the JET-ILW support the expectation of a strong impact of the DSL upon the H_α (and Visible Light) Spectroscopy Diagnostic in ITER. In ITER, one may expect stronger DSL because, at least, of the obviously higher reflectivity of the first wall on the low-field side.

The estimation of the neutral atom density in the SOL can be done with the developed algorithms provided the absolute calibration of all the signals is available. The bifurcated-LoS measurement scheme [4] suggested for ITER (namely, targeting at an optical dump and very close to it) cannot be tested now on JET for technical reasons. The present application of synthetic diagnostic algorithms for ITER to JET-ILW was limited to evaluation of the accuracy of recovering the DSL/SOLL ratio. The validation of the bifurcated-LOS scheme in JET-ILW experiments would be very helpful for all ITER diagnostics in the visible light range. Also, generation of synthetic data for JET would be very helpful for testing the algorithms suggested for measurement accuracy evaluation in ITER.

Acknowledgements. This work was supported by the RF State Corporation Rosatom and Euratom, and carried out within the framework of the cooperation between EUROfusion Consortium and Rosatom. This work has been carried out within the framework of the EUROfusion Consortium and has received funding from the Euratom research and training programme 2014-2018 under grant agreement No 633053. The authors thank E.N. Andreenko, A.V. Gorshkov, M.B. Kadomtsev, V. Kotov, A.S. Kukushkin, M.G. Levashova, S.W. Lisgo, V.S. Lisitsa, V.A. Shurygin, E. Veshchev, D.K. Vukolov, K.Yu. Vukolov for their collaboration in studies on the ITER Main Chamber H-alpha (and Visible Light) Spectroscopy.

Disclaimer: The views and opinions expressed herein do not necessarily reflect those of the European Commission and ITER Organization.

References

[1] Donné A J H et al 2007 *Nucl. Fusion* **47** (6) S337-84

[2] Harhausen J, Kallenbach A and Fuchs C and the ASDEX Upgrade Team 2011 *Plasma Phys. Control. Fusion* **53** (2) 025002-22
[3] Harhausen J 2008 Interpretation of D_α Imaging Diagnostics Data on the ASDEX Upgrade Tokamak *PhD thesis* (Ludwig-Maximilian University Munich)
[4] Kukushkin A B et al 2012 *Proc. 24th IAEA FEC* (*San Diego, USA, 8-13 October 2012*) ITR/P5-44
[5] Kajita S et al 2013 *Plasma Phys. Contr. Fusion* **55** (8) 085020-8
[6] Kukushkin A S, Pacher H D, Kotov V, Pacher G W and Reiter D 2011 *Fusion Eng. Des.* **86** (12) 2865-73
[7] Braams B J 1986 Computational studies in tokamak equilibrium and transport *PhD thesis* (Utrecht: Rijksuniversitet)
[8] Reiter D, Baelmans M and Börner P 2005 *Fusion Sci. Tech.* **47** (2) 172-86
[9] Lisgo S W, Börner P, Kukushkin A, Pitts R A, Polevoi A and Reiter D 2011 *J. Nucl. Mater.* **415** (1) S965-68
[10] Kukushkin A B, Neverov V S, Alekseev A G, Lisgo S W and Kukushkin A S 2016 *Fusion Sci. Tech.* **69** (3) 628-42
[11] Kukushkin A B, Neverov V S, Kadomtsev M B, Kotov V, Kukushkin A S, Levashova M G, Lisgo S W, Lisitsa V S, Shurygin V A and Alekseev A G 2014 *Journal of Physics: Conference Series*, **548** 012012
[12] Neverov V S, Kukushkin A B, Lisgo S W, Kukushkin A S and Alekseev A G 2015 *Plasma Phys. Rep.* **41** (2) 103-11
[13] Kadomtsev M B, Kotov V, Lisitsa V S and Shurygin V A 2012 *Proc. 39th EPS Conference & 16th Int. Congress on Plasma Physics (Stockholm, Sweden, 2-6 July 2012)* P4.093
[14] Lisitsa V S, Kadomtsev M B, Kotov V, Neverov V S and Shurygin V A 2014 *Atoms* **2** (2) 195-206
[15] Kukushkin A B et al 2014 *AIP Conference Proceedings* **1612** 97-100
[16] Kukushkin A B et al 2014 *Proc. 25th IAEA Fusion Energy Conf. (St. Petersburg, Russia, 13-18 October 2014)* EX/P5-20 (Preprint EFDA–JET–CP(14)06/33 http://www.euro-fusionscipub.org/wp-content/uploads/2015/04/EFDC140633.pdf)
[17] Lomanowski B A, Meigs A G, Sharples R M, Stamp M, Guillemaut C and JET Contributors 2015 *Nucl. Fusion* **55** 123028-42
[18] Andreenko E N, Alekseev A G, Kukushkin A B, Neverov V S, Lisgo S W and Morozov A A 2016 Optimization of optical dumps for H-alpha spectroscopy in ITER *Submitted to 29th Symposium on Fusion Technology (Prague, Czech Republic, 5-9 September 2016)*
[19] Lao L L, John H St, Stambaugh R D and Pfeiffer W 1985 *Nucl. Fusion* **25** (10) 1421-35